


Article

Study and Comparison of Hyperbolic and Pseudorange Positioning Algorithms in the eLoran System

Man Yang ^{1,2}, Baorong Yan ¹, Chaozhong Yang ¹ , Wei Guo ¹ and Shifeng Li ^{1,2,*}

¹ National Time Service Center, Chinese Academy of Sciences, Xi'an 710600, China; yangman@ntsc.ac.cn (M.Y.); yanbaorong@ntsc.ac.cn (B.Y.); ycz@ntsc.ac.cn (C.Y.); guowei@ntsc.ac.cn (W.G.)

² University of Chinese Academy of Sciences, Beijing 100049, China

* Correspondence: lishifeng@ntsc.ac.cn; Tel.: +86-029-83890360

Abstract: The positioning algorithms of the Enhanced Long-Range Navigation (eLoran) system primarily include the hyperbolic positioning algorithm and the pseudorange positioning algorithm. However, the calculations present in the existing literature are inaccurate and lack empirical data, and a thorough and precise comparison of the two algorithms has yet to be conducted. Therefore, this paper employs a combination of simulation analysis and empirical analysis to explore these two positioning algorithms in depth, with an optimization of the initial position calculation in the pseudorange algorithm. Under ideal conditions without observational errors, through precise calculations and analysis, the positioning errors of both algorithms are approximately zero, and full-area solutions can be achieved. Under conditions with observational errors, this study shows that both algorithms exhibit positioning errors, with the pseudorange algorithm achieving a level of accuracy comparable to that of the hyperbolic algorithm. At the same time, the empirical analysis further verified this conclusion. Additionally, this study found that the pseudorange positioning algorithm demonstrated better applicability in practical applications, as it successfully resolved the multivalued and singularity issues present in the hyperbolic positioning algorithm.

Keywords: eLoran; hyperbolic positioning algorithm; pseudorange positioning algorithm; positioning accuracy



Citation: Yang, M.; Yan, B.; Yang, C.; Guo, W.; Li, S. Study and Comparison of Hyperbolic and Pseudorange Positioning Algorithms in the eLoran System. *Electronics* **2024**, *13*, 3986. <https://doi.org/10.3390/electronics13203986>

Academic Editor: Maciej Ławryńczuk

Received: 24 August 2024

Revised: 20 September 2024

Accepted: 8 October 2024

Published: 10 October 2024



Copyright: © 2024 by the authors. Licensee MDPI, Basel, Switzerland. This article is an open access article distributed under the terms and conditions of the Creative Commons Attribution (CC BY) license (<https://creativecommons.org/licenses/by/4.0/>).

1. Introduction

The Global Navigation Satellite System (GNSS) is currently the most widely used navigation system. However, due to its weak signals, it is vulnerable to interference, making it susceptible to certain limitations and weaknesses. To address this issue, the Enhanced Long-Range Navigation (eLoran) system, a terrestrial radio navigation system, has gained increasing attention. Built on the foundation of the traditional Loran-C system, eLoran offers enhanced anti-jamming capabilities, broader coverage, and higher reliability, making it a critical complement and backup to GNSS, particularly in scenarios where GNSS signals face interference, obstruction, or malicious attacks. Although eLoran's positioning accuracy is generally inferior to GNSS, modern advancements in technologies such as transmission systems, differential techniques, and precise time synchronization have significantly improved its accuracy [1,2]. This allows eLoran to provide reliable Positioning, Navigation, and Timing (PNT) services.

The traditional Loran-C system uses the hyperbolic positioning algorithm, which eliminates the clock bias between the receiver and the system. On this basis, various computational methods have also been developed, such as cross-chain and additional constraint conditions [3–5]. In recent years, the system has undergone upgrades and modifications, developing into the eLoran system. The most obvious improvement is that all eLoran signals can be related to a common time reference, and thus, pseudorange measurements are available for all transmitters [6]. As a result, the pseudorange positioning

algorithm can be used for positioning calculations. This algorithm is not constrained by station chains, making it more flexible and commonly used in integrated navigation systems [7–11].

However, the positioning accuracy of the eLoran system has certain limitations. To overcome this, some studies have proposed improving accuracy by correcting propagation delays [12–16], while also exploring various enhancement methods [17–19]. The majority of the research focuses on the analysis of Dilution of Precision (DOP) values and the conditions of the forward operating area [20–22] but has overlooked the accuracy analysis of the hyperbolic positioning algorithm and pseudorange positioning algorithm themselves. Even under ideal conditions without observational errors, the computational accuracy of these two algorithms across the entire area has not been fully revealed. Most studies suggest that the positioning errors of both algorithms are at the meter level [23,24]. However, research conducted by Yan et al. found that the positioning error of the pseudorange positioning algorithm can reach millimeter-level accuracy [25].

Furthermore, the pseudorange positioning algorithm may encounter convergence errors when reliable initial position information is lacking. To address this issue, many scholars use the initial position derived from the hyperbolic positioning algorithm as the initial value for the pseudorange positioning algorithm, thus making the pseudorange positioning algorithm somewhat dependent on the hyperbolic positioning algorithm. Liu et al. proposed a branch and bound algorithm based on interval contraction, which effectively resolves the initialization problem of the pseudorange positioning algorithm [26,27]. Although this algorithm is complex, it provides an effective solution.

Despite the existing research foundation, comparative studies of the two positioning algorithms remain insufficient. Most of the literature relies on simulation analysis, which, while helpful for research, fails to accurately reflect the impact of eLoran groundwave signal propagation errors on positioning accuracy in real-world environments. Some studies have adopted empirical analysis methods, but due to experimental constraints, they are typically limited to one or two measured points, which makes the findings less convincing.

Therefore, this paper will conduct a thorough study and comparison of the hyperbolic positioning and pseudorange positioning algorithms of the eLoran system using a method combining simulation and empirical analysis. In the simulation analysis, the performance of the algorithms will be analyzed under both conditions, with and without observation errors. Under conditions without observational errors, by utilizing a search method to solve for unknown variables and applying suitable convergence thresholds, the positioning errors of the two algorithms are further minimized and clarified, and full-area solutions can be achieved. Additionally, a simpler mathematical geometric method is applied to solve the initial value problem in the pseudorange positioning algorithm, thereby simplifying the algorithm. Under conditions with observational errors, the impact of different sources of errors on the positioning accuracy of two algorithms was studied, and a comparison of the two algorithms was conducted. Finally, calculations and analyses of empirical data further verify the conclusions drawn from the simulation analysis.

2. Hyperbolic Positioning Algorithm

The eLoran system typically uses the hyperbolic positioning algorithm for positioning. This algorithm requires at least one single chain, which consists of one master station and two secondary stations. The receiver captures signals transmitted from the master and secondary stations of the same chain and measures the time differences between the secondary stations relative to the master station. Under the condition of a constant signal propagation speed, the time differences can be converted into distance differences. Using the mathematical definition of a hyperbola, the distance difference between a moving point and two fixed points is a constant value, which allows for the drawing of a hyperbola with these two fixed points as foci. Based on two time differences, two intersecting hyperbolas can be drawn, and one of the intersection points of the hyperbolas is the receiver's location.

The hyperbolic positioning algorithm consists of two parts. The first part involves calculating the initial position, which is the receiver's rough location. The Earth is simplified into a perfect sphere, and distances are calculated on the sphere's surface to determine the initial position. The second part calculates the precise position by performing Newton's iteration on the ellipsoidal surface based on the initial position. The final result of the iteration is the precise position of the receiver.

2.1. Solve for the Initial Position

The geometric relationships of the hyperbolic positioning algorithm are shown in Figure 1. Station 2 is the leader station, and Stations 1 and 3 are the two secondary stations, with their coordinates being (φ_2, λ_2) , (φ_1, λ_1) , and (φ_3, λ_3) , respectively. Point P is the location of the receiver, and its coordinates are the unknown variable (φ, λ) . β_1 is the azimuth angle from Station 1 to Station 2, β_3 is the azimuth angle from Station 3 to Station 2, and θ is the azimuth angle from the receiver point P to Station 2. d_1 is the spherical distance between Station 1 and Station 2, d_3 is the spherical distance between Station 3 and Station 2, and ρ_1 , ρ_2 , and ρ_3 are the spherical distances from Stations 1, 2, and 3 to the receiver, respectively. The spherical distances are measured in radians.

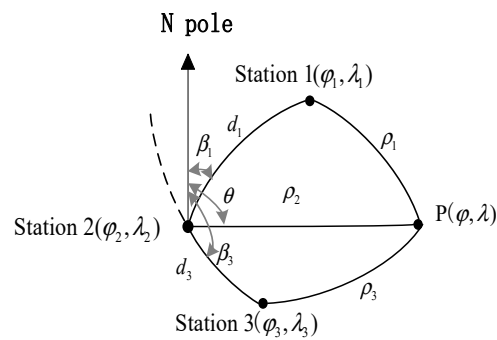


Figure 1. The geometric relationships of the hyperbolic positioning algorithm.

Based on the geometric relationship diagram above, the following system of formula is established using the spherical triangle cosine law and the principles of hyperbolic positioning [23].

$$\begin{cases} \cos \rho_1 = \cos d_1 \cos \rho_2 + \sin d_1 \sin \rho_2 \cos(\theta - \beta_1) \\ \cos \rho_3 = \cos d_3 \cos \rho_2 + \sin d_3 \sin \rho_2 \cos(\theta - \beta_3) \\ \rho_1 - \rho_2 = \zeta_1 \\ \rho_3 - \rho_2 = \zeta_2 \end{cases}, \quad (1)$$

where ζ_1 and ζ_2 represent the spherical distance differences between the receiver and the leader and secondary stations, which can be obtained using the formula $\zeta_i = \Delta T_i \times c/a$, where ΔT_i is the known time difference, c is the speed of electromagnetic waves in the air, and a is the length of the Earth's semi-major axis. The unknown variables are ρ_1 , ρ_2 , ρ_3 , and θ .

This paper simplifies and integrates the formula for solving. When solving the unknown variable θ in the system formula, a search method is applied, where values satisfying the conditions are obtained through an iterative search. The search step is 0.0001 degrees, which is equivalent to 0.36 arcseconds, corresponding to 10.8 m. Compared to directly solving the formula, the search method offers greater flexibility and adaptability, avoiding the complexity of solving via trigonometric functions. However, since the system of the formula does not have a unique solution, it is necessary to first determine whether point P is located in the front or back region and, accordingly, set a reasonable search range for θ . Once θ is determined, the remaining three unknowns can be easily solved. After converting the solved θ and ρ_2 , the spherical latitude and longitude can be obtained, representing the initial location (φ_0, λ_0) .

2.2. Solve for the Precise Position

After approximately determining the receiver's position, the Newton iteration method is applied on the ellipsoidal surface to correct the initial position, using the coordinates of the leader and secondary stations and the time differences. When the iteration converges to a certain extent, the resulting coordinates are the precise position of the receiver.

ξ_1 and ξ_2 are continuous bivariate functions with respect to the unknown point (φ, λ) , where (φ, λ) represent the spherical latitude and longitude coordinates. The following system of formula is established.

$$\begin{cases} \xi_1 = F_1(\varphi, \lambda) \\ \xi_2 = F_2(\varphi, \lambda) \end{cases}, \quad (2)$$

The function $F(\varphi, \lambda)$ represents the spherical distance differences between point (φ, λ) and the leader and secondary stations, with units in radians. Given the initial position (φ_0, λ_0) , the corresponding spherical distance differences in radians, denoted as ξ_1^0 and ξ_2^0 , can be calculated and satisfy the equation.

$$\begin{cases} \xi_1^0 = F_1(\varphi_0, \lambda_0) \\ \xi_2^0 = F_2(\varphi_0, \lambda_0) \end{cases}, \quad (3)$$

Expand the system of Formula (2) using a Taylor series around the initial position (φ_0, λ_0) , neglecting higher-order terms. The positional deviation $(\Delta\varphi, \Delta\lambda)$ between the true position (φ, λ) and the initial position (φ_0, λ_0) is represented by $\Delta\varphi = \varphi - \varphi_0$, $\Delta\lambda = \lambda - \lambda_0$. The final system of equations is as follows:

$$\begin{cases} \xi_1 - \xi_1^0 = \frac{\partial \xi_1}{\partial \varphi} \Delta\varphi + \frac{\partial \xi_1}{\partial \lambda} \Delta\lambda \\ \xi_2 - \xi_2^0 = \frac{\partial \xi_2}{\partial \varphi} \Delta\varphi + \frac{\partial \xi_2}{\partial \lambda} \Delta\lambda \end{cases}, \quad (4)$$

where ξ_1 and ξ_2 are the spherical distance differences derived from the time differences measured by the receiver. ξ_1^0 and ξ_2^0 are the geodetic distance differences between the initial position (φ_0, λ_0) and the leader and secondary stations, divided by the Earth's semi-major axis. The Andoyer–Lambert formula is used to calculate the geodetic distances on the ellipsoidal surface, as shown in Equation (3). By calculating the partial derivatives at the initial position (φ_0, λ_0) , the position error $\Delta\varphi$ and $\Delta\lambda$ can be solved.

The iteration process corrects the initial position using the positional deviations $\Delta\varphi$ and $\Delta\lambda$, resulting in new initial coordinates $\varphi_0 = \varphi_0 + \Delta\varphi$, $\lambda_0 = \lambda_0 + \Delta\lambda$. The new initial position is then substituted back into the formula, and the process is repeated. When the absolute values of the positional deviations are smaller than the predetermined convergence threshold, the calculation is complete, and the resulting position is the precise position of the receiver. Finally, this precise position is converted from spherical latitude and longitude to ellipsoidal latitude and longitude, yielding the receiver's precise geodetic coordinates (B, L) .

3. Pseudorange Positioning Algorithm

The pseudorange positioning algorithm eliminates the dependency on the station chain in the hyperbolic positioning algorithm. However, the pseudorange contains the clock bias between the receiver and the eLoran system, which cannot be eliminated and must be treated as an unknown to be solved. Along with the receiver's latitude and longitude, a total of three unknown variables need to be solved, requiring at least three stations, though they do not need to be within the same chain. The receiver receives signals from each station and measures the propagation time delay of each signal to the receiver, which is then used to calculate the distance between the receiver and each station [28]. With each station as a center and the distance between each station and the receiver as the radius, circles are drawn, and the intersection of the arcs is the location of the receiver, with only one intersection point existing.

The pseudorange positioning algorithm also consists of two parts: calculating the initial position and calculating the precise position.

3.1. Solve for the Initial Position

Its geometric relationship diagram is the same as that shown in Figure 1, and the following system of the formula can be established using the spherical triangle cosine rule.

$$\begin{cases} \cos \rho_1 = \cos d_1 \cos \rho_2 + \sin d_1 \sin \rho_2 \cos(\theta - \beta_1) \\ \cos \rho_3 = \cos d_3 \cos \rho_2 + \sin d_3 \sin \rho_2 \cos(\theta - \beta_3) \end{cases} \quad (5)$$

This system of formula contains only one unknown, yet it is constrained by two formulae. In this case, the multivalued nature of the sine and cosine functions will not pose an obstacle to the solution, nor will it lead to multiple solutions. During the solution process, the search method is similarly applied, with a search step of 0.0001° , and the search range is from 0° to 360° , allowing for the solution across the full-area. Once θ is found, the initial position (φ_0, λ_0) can be easily obtained.

3.2. Solve for the Precise Position

After obtaining the initial position, the ellipsoidal pseudorange positioning algorithm is applied, iterating on the ellipsoidal surface. The positioning equation based on the pseudorange can be simplified as follows:

$$D_i = L_i - t_u \cdot c, \quad (6)$$

where D_i represents the pseudorange value from a certain station to the receiver. L_i represents the geodetic distance between the station and the receiver; the geodetic distance between two points is calculated using the Andoyer–Lambert formula [29]. t_u represents the clock bias between the station signal and the receiver. Let the receiver's initial position be $(\varphi_0, \lambda_0, t_{u0})$, where (φ_0, λ_0) is the initial position obtained earlier, and set the initial clock bias $t_{u0} = 0$. Expanding this Equation at the initial position using a Taylor series and neglecting the higher-order terms, the following system of formula can be established.

$$\begin{cases} D_1 - L_{10}(\varphi_0, \lambda_0, t_{u0}) + t_{u0} \times c = \frac{\partial D_i}{\partial \varphi} \bigg|_{L_{10}} \Delta \varphi + \frac{\partial D_i}{\partial \lambda} \bigg|_{L_{10}} \Delta \lambda + \frac{\partial D_i}{\partial t_u} \bigg|_{L_{10}} \Delta t_u \\ D_2 - L_{20}(\varphi_0, \lambda_0, t_{u0}) + t_{u0} \times c = \frac{\partial D_i}{\partial \varphi} \bigg|_{L_{20}} \Delta \varphi + \frac{\partial D_i}{\partial \lambda} \bigg|_{L_{20}} \Delta \lambda + \frac{\partial D_i}{\partial t_u} \bigg|_{L_{20}} \Delta t_u \\ D_3 - L_{30}(\varphi_0, \lambda_0, t_{u0}) + t_{u0} \times c = \frac{\partial D_i}{\partial \varphi} \bigg|_{L_{30}} \Delta \varphi + \frac{\partial D_i}{\partial \lambda} \bigg|_{L_{30}} \Delta \lambda + \frac{\partial D_i}{\partial t_u} \bigg|_{L_{30}} \Delta t_u \end{cases} \quad (7)$$

where, D_1, D_2 , and D_3 are the pseudorange values measured by the receiver. The pseudorange positioning equation can then be organized into the following form.

$$B = A \cdot X, \quad (8)$$

where

$$B = \begin{bmatrix} D_1 - L_{10}(\varphi_0, \lambda_0, t_{u0}) + t_{u0} \times c \\ D_2 - L_{20}(\varphi_0, \lambda_0, t_{u0}) + t_{u0} \times c \\ D_3 - L_{30}(\varphi_0, \lambda_0, t_{u0}) + t_{u0} \times c \end{bmatrix}, \quad A = \begin{bmatrix} \frac{\partial D_i}{\partial \varphi} \bigg|_{L_{10}} & \frac{\partial D_i}{\partial \lambda} \bigg|_{L_{10}} & \frac{\partial D_i}{\partial t_u} \bigg|_{L_{10}} \\ \frac{\partial D_i}{\partial \varphi} \bigg|_{L_{20}} & \frac{\partial D_i}{\partial \lambda} \bigg|_{L_{20}} & \frac{\partial D_i}{\partial t_u} \bigg|_{L_{20}} \\ \frac{\partial D_i}{\partial \varphi} \bigg|_{L_{30}} & \frac{\partial D_i}{\partial \lambda} \bigg|_{L_{30}} & \frac{\partial D_i}{\partial t_u} \bigg|_{L_{30}} \end{bmatrix}, \quad X = \begin{bmatrix} \Delta \varphi \\ \Delta \lambda \\ \Delta t_u \end{bmatrix}$$

Using the least squares method, the system of formula can be solved, yielding

$$X = (A^T A)^{-1} \cdot (A^T B), \quad (9)$$

The solution vector $\Delta \varphi, \Delta \lambda, \Delta t_u$ represents the deviation values. Once these deviations are determined, the position can be corrected. The new position is then substituted back

into the formula for further iteration. This process is repeated until the absolute values of the deviations are smaller than the predefined convergence threshold. After the calculation process is completed, the final position is converted from spherical coordinates to ellipsoidal coordinates. The output position is the receiver's precise location and the clock bias value that satisfies the conditions.

4. Simulation Analysis

To compare the positioning accuracy of the two algorithms, latitude and longitude positioning error is used as a metric, meaning the difference between the calculated position and the true position.

This paper uses the Nanhai station chain as an example for simulation analysis. The leader station is located in Hezhou, Guangxi, with secondary stations located in Raoping, Guangdong, and Chongzuo, Guangxi. The analysis is divided into two categories based on the presence or absence of observational errors.

In the case without observational errors, the time difference is the difference in the geodesic distances on the ellipsoidal surface between the receiver and the leader and secondary stations, while the pseudorange is the geodesic distance on the ellipsoidal surface between the receiver and the station. The positioning error reflects the inherent error of the algorithm itself.

In the case with observational errors, the time difference is the sum of the geodesic distance difference on the ellipsoidal surface between the receiver and the leader and secondary stations and the observational error. The pseudorange is the sum of the geodesic distance between the receiver and the station on the ellipsoidal surface and the observational error. The positioning error in this case reflects the impact of observational errors on positioning accuracy.

The simulation environment in this paper is based on Matlab R2023b, running on the Windows 11 operating system, with hardware featuring an Intel Core Ultra 7 155H processor and 32 GB of memory to ensure efficient and accurate simulation calculations.

This paper simulated the latitude and longitude positioning within a specific region and converted the positioning errors into distance measurements, quantified in meters. The simulation covered the area within a latitude range of 18° to 28° and a longitude range of 102° to 122° . The simulation was performed with a step size of 0.5 degrees.

4.1. No Observational Errors

Under ideal conditions without observational errors, the positioning error is determined by the inherent computational accuracy of the algorithms. To improve the performance of both algorithms, this paper first conducted numerous repeated experiments to explore the best solution methods and optimal iterative convergence thresholds. After careful adjustments and testing, both algorithms achieved high levels of computational accuracy. Subsequently, to comprehensively assess the algorithms' accuracy and avoid the influence of isolated outliers, a large-scale simulation analysis was carried out.

4.1.1. Hyperbolic Positioning Algorithm

First, the approximate region of the receiver is estimated to determine whether it is in the forward or backward zone. Next, the necessary time difference data are simulated. During this process, based on the coordinates of each station and the receiver, the distances between each station and the receiver on the ellipsoid surface are calculated. These distance differences are then converted into time differences by considering the speed of electromagnetic wave propagation. Finally, the hyperbolic positioning algorithm is applied to solve for the receiver's coordinate position.

In the calculation, the key condition for convergence is that the absolute values of the deviation $\Delta\varphi$, $\Delta\lambda$ are both less than the set convergence threshold. Through extensive experimental research and data analysis, this paper sets the convergence threshold of the hyperbolic positioning algorithm at 10^{-9} degrees, which corresponds to a distance

error of 0.1 mm. In most cases, the iterative process converges after about four iterations. Increasing the convergence threshold does not significantly affect the positioning results, while lowering the threshold may degrade the results. This iterative threshold strikes a good balance between positioning accuracy and computational efficiency. In the subsequent experiments with the hyperbolic positioning algorithm, this convergence threshold is consistently used to ensure the reliability and consistency of the results. Additionally, considering that some regional points may not meet the preset convergence condition, a limit is set so that if the number of iterations exceeds 50, the process will automatically exit the loop.

In the simulation area, to avoid the negative impact of excessively large positioning errors on the overall results, the error range is constrained, and points with errors larger than 10^{-4} are discarded. Then, the remaining regional points are analyzed and displayed in detail. The latitude and longitude error results of the hyperbolic positioning algorithm for this region are shown in Figure 2.

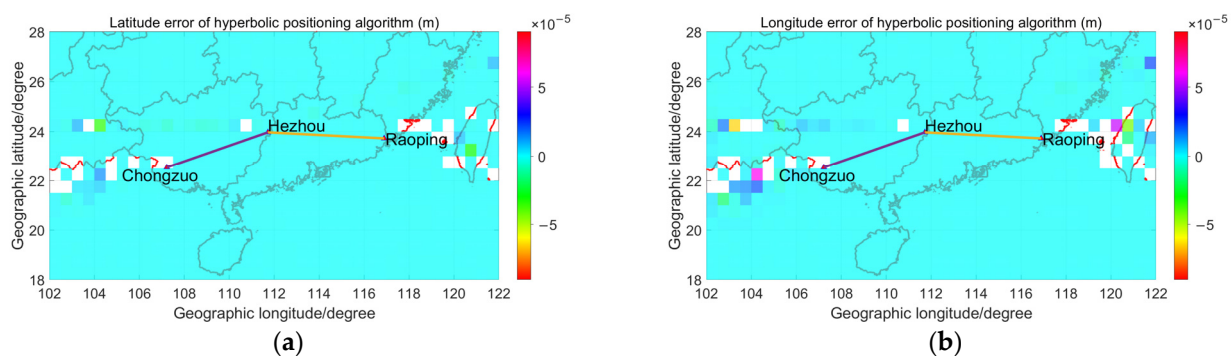


Figure 2. Hyperbolic positioning results when there is no observation error: (a) latitude error; (b) longitude error.

From the simulation result maps, it can be observed that under ideal conditions without observational errors, the hyperbolic positioning algorithm successfully computes the position for most of the region and achieves high-precision results, with positioning errors approaching zero. However, when the positioning point is located near the extension or reverse extension of the two baseline lines, singularity issues occur, leading to errors in the positioning calculations.

4.1.2. Pseudorange Positioning Algorithm

To simplify the research process, the clock offset between the receiver and the eLoran system is set to zero. During the calculation, there are no multiple-value situations, so there is no need to determine the approximate region where the receiver is located. Subsequently, based on the coordinates of each station and the user point, and using the geodetic distance calculation formula, the pseudorange values measured by the receiver are simulated. Finally, using simulation data, the pseudorange positioning algorithm is applied to solve for the receiver's coordinate position.

In the calculations, the key condition for convergence is that the absolute values of the deviation values $\Delta\varphi$, $\Delta\lambda$, Δt_u are all less than the set convergence threshold. Through extensive repeated experimental studies, this paper sets the convergence threshold for the pseudorange positioning algorithm at 10^{-11} degrees, with approximately four iterations needed to achieve good positioning results and reduce redundant calculations. In the subsequent pseudorange positioning algorithm experiments, this convergence threshold is consistently used to ensure the reliability and consistency of the results. Additionally, considering that some regional points may not meet the preset convergence conditions, a limit is set so that if the number of iterations exceeds 50, the process will automatically exit the loop.

In the simulation area, to avoid the negative impact of excessively large positioning errors on the overall results, the error value range is restricted. Points with errors greater than 10^{-4} are discarded, and the remaining regional points are displayed and analyzed in detail. The latitude and longitude error results for the pseudorange positioning algorithm in this region are shown in Figure 3.

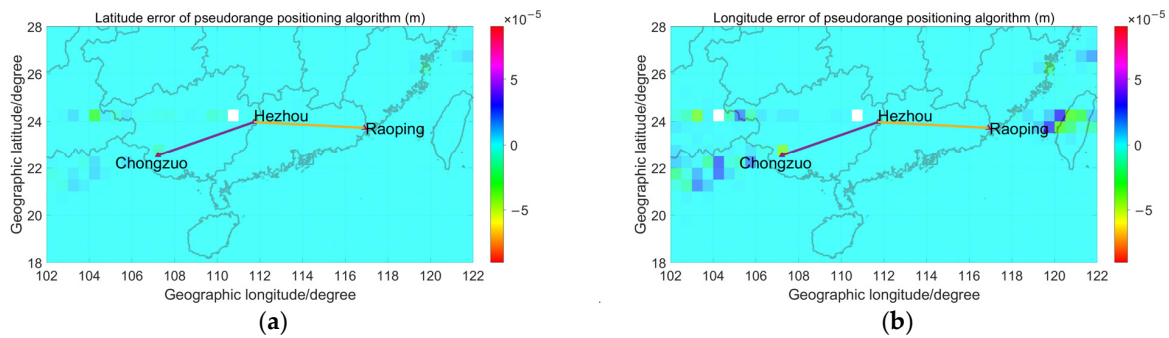


Figure 3. Pseudorange positioning results when there is no observation error: (a) latitude error; (b) longitude error.

From the simulation result maps, it can be observed that under ideal conditions without observational errors, the pseudorange positioning algorithm successfully solves all regions and achieves high-precision positioning, with positioning errors close to zero. Additionally, the pseudorange positioning algorithm resolves the singularity issues encountered in the hyperbolic positioning algorithm. The two uncolored points in Figure 3 do not indicate the occurrence of singularity issues, but rather their positioning error is 10^{-3} , exceeding the range set by the current data display limits.

4.2. Observational Errors

In the simulation analysis in Section 4.1, it can be seen that both algorithms achieve high positioning accuracy in the absence of observational errors. However, eLoran signals are influenced by various factors during transmission, leading to observational errors in the time differences and pseudoranges measured by the receiver, which affects the positioning results and introduces deviations. To explore the impact of observational errors on different algorithms, observational errors were divided into systematic and random errors. Four representative points were selected for simulation analysis, as shown in Figure 4, and an accurate comparison of the positioning error results was conducted. Subsequently, a positioning error map was plotted, and the analysis was carried out across the entire plane.

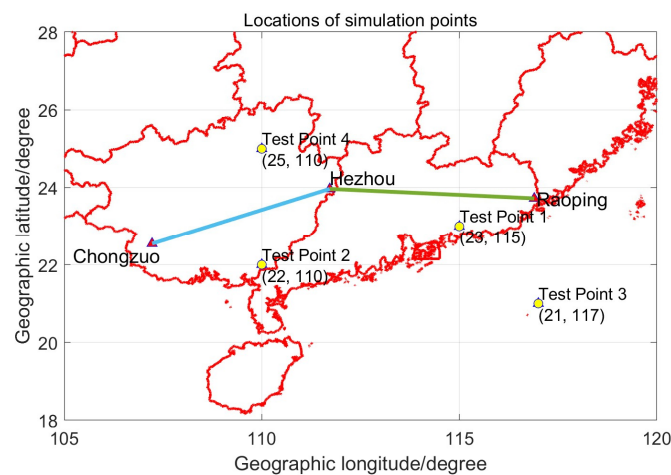


Figure 4. Locations of simulation points.

4.2.1. Systematic Errors

The signal propagation speed is influenced by factors such as the air refractive index, ground dielectric constant, and conductivity along the propagation path. Additionally, terrain variations along the propagation path mean that the propagation time does not precisely correspond to the propagation distance, all of which contribute to systematic errors.

When the systematic error caused by the terrain is not considered, in order to simulate the time differences and pseudoranges containing systematic errors, a fixed systematic error of 200 ns, 150 ns, and 180 ns was added to the propagation time from the Hezhou leader station, the Raoping secondary station, and the Chongzuo secondary station to the receiver at each test point, respectively. Subsequently, detailed calculations were then performed. The positioning error results of each simulation point are summarized in Table 1.

Table 1. Positioning error results when the systematic errors are overlaid based on a fixed value.

Method	Test Points	Positioning Error (m)
Hyperbolic Positioning Algorithm	1	(−17.82, 9.19)
	2	(−25.68, 5.83)
	3	(−32.03, 38.83)
	4	(42.49, −8.33)
Pseudorange Positioning Algorithm	1	(−17.82, 9.19)
	2	(−25.68, 5.83)
	3	(−32.03, 38.83)
	4	(42.49, −8.33)

At the same time, the positioning error across the entire simulation range was generated, as shown in Figures 5 and 6. Due to the high DOP values in the intersection areas of the baselines and their extended lines, this region exhibits more significant positioning errors compared to other areas when the same observational error is introduced. When the data span a wide range, plotting may cause data points with vastly different values to appear in similar colors, making it difficult to distinguish between them, affecting the observation results. To better illustrate this, only data points with absolute error values less than 1000 were displayed, ensuring that each point in the plot clearly and accurately reflects its true positioning error.

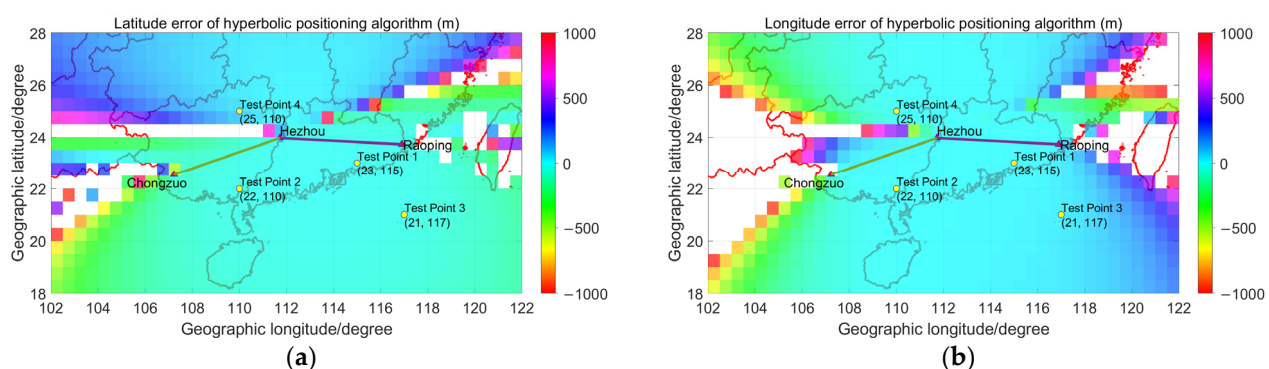


Figure 5. Hyperbolic positioning results when the systematic errors are overlaid based on a fixed value: (a) latitude error; (b) longitude error.

Furthermore, considering the fact that systematic errors may be related to signal propagation distance, different systematic errors were added to the propagation delays for each simulation point based on distance, with the errors being calculated using the Lagrange interpolation method. These values were derived from the approximate conditions of the average terrestrial path of 100 kHz ground wave secondary delay (radiated power $P = 1$ kW) according to the document [30]. The specific details are shown in Table 2.

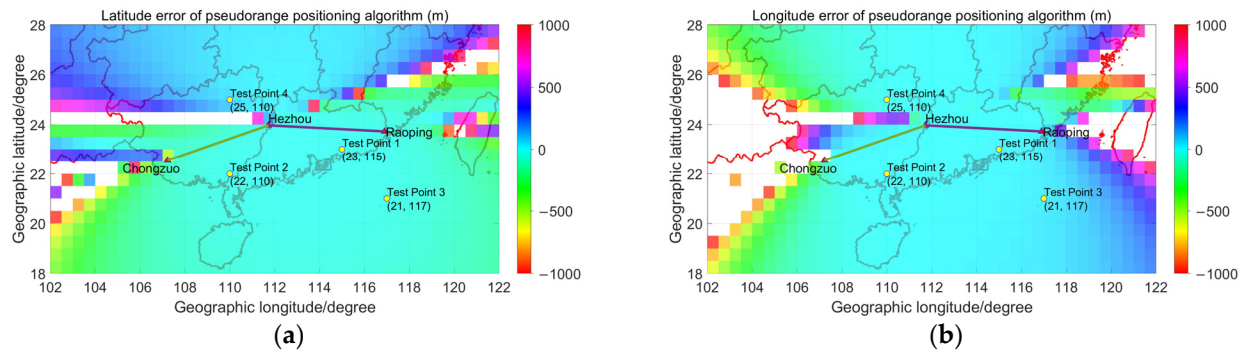


Figure 6. Pseudorange positioning results when the systematic errors are overlaid based on a fixed value: (a) latitude error; (b) longitude error.

Table 2. Systematic error overlay.

Test Points	Hezhou (μ s)	Raoping (μ s)	Chongzuo (μ s)
1	3.1	2.3	5.5
2	2.7	5.1	2.8
3	4.6	2.8	6.8
4	2.0	4.7	3.0

Subsequently, detailed calculations were performed. The positioning error results of each simulation point are summarized in Table 3.

Table 3. Positioning error results when the systematic errors are overlaid based on the distances.

Method	Test Points	Positioning Error (m)
Hyperbolic Positioning Algorithm	1	(1992.95, 52.90)
	2	(1149.07, −416.36)
	3	(2159.28, −634.99)
	4	(−2299.92, 435.70)
Pseudorange Positioning Algorithm	1	(1992.95, 52.90)
	2	(1149.07, −416.36)
	3	(2159.28, −634.99)
	4	(−2299.92, 435.70)

At the same time, the positioning error across the entire simulation range was generated, as shown in Figures 7 and 8. Due to the significant overlay of systematic errors, only data points with absolute error values of less than 10,000 were displayed.

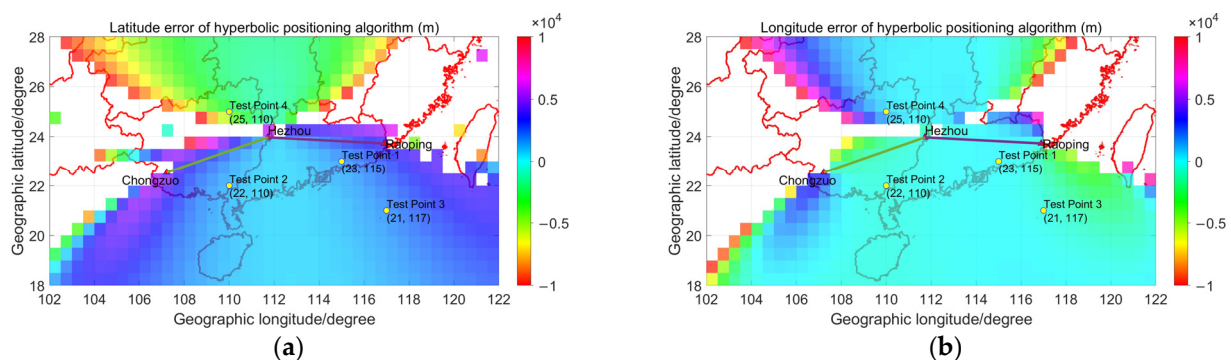


Figure 7. Hyperbolic positioning results when systematic errors are overlaid based on the distances: (a) latitude error; (b) longitude error.

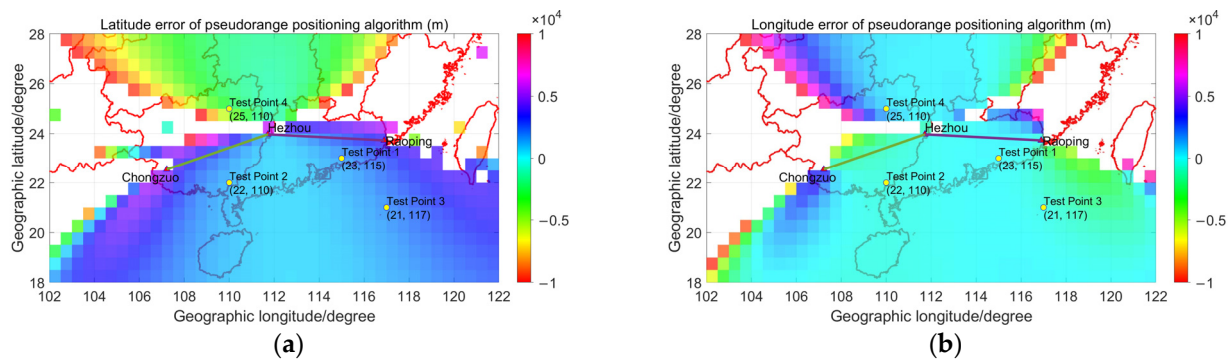


Figure 8. Pseudorange positioning results when systematic errors are overlaid based on the distances: (a) latitude error; (b) longitude error.

From Tables 1 and 3, it can be seen that when systematic errors are present, the positioning results are affected, resulting in increased positioning errors. Both algorithms have certain longitude and latitude positioning errors, and the errors are comparable. From Figures 5–8, a similar conclusion can be drawn, as the positioning error plots for both algorithms are alike, with differences only being seen at a few points.

4.2.2. Random Errors

In addition to systematic errors, random errors caused by factors such as noise and weather also affect positioning. Random errors tend to follow a Gaussian distribution. Therefore, the MATLAB function `randn` was used to generate a random sequence, and $0.5 \times \text{randn} \mu\text{s}$ were added to the signal propagation delays from each station to the receiver. Each test point was calculated and statistically analyzed 1000 times with different random errors. After calculations, the average values and standard deviations of the longitude and latitude positioning errors for each test point were compiled, as shown in Table 4. Since simulating the entire area requires an enormous amount of computation, the paper chooses not to present the result in graphical form.

Table 4. Positioning error results when the random errors are overlaid.

Method	Test Points	Positioning Error (m)	Standard Deviation (m)
Hyperbolic Positioning Algorithm	1	(1992.95, 52.90)	(608.29, 132.49)
	2	(1149.07, −416.36)	(370.83, 117.24)
	3	(2159.28, −634.99)	(864.48, 725.80)
	4	(−2299.92, 435.70)	(599.66, 187.32)
Pseudorange Positioning Algorithm	1	(1992.95, 52.90)	(608.29, 132.50)
	2	(1149.07, −416.36)	(370.83, 117.24)
	3	(2159.28, −634.99)	(864.48, 725.80)
	4	(−2299.92, 435.70)	(599.66, 187.32)

From Table 4, a similar conclusion can be drawn: when random errors are present, they will affect the positioning results, leading to increased positioning errors. Both algorithms exhibit certain latitude and longitude positioning errors, and the errors are similar.

5. Empirical Analysis

Although simulations can be used to study and compare the two different positioning algorithms of the eLoran system from various angles, the results often differ from the empirical data. These discrepancies may stem from multiple factors, including the simplified assumptions in the simulation model, the complexity of environmental variables, and uncertainties that were not considered in the empirical measurements. Empirical data reflect the combined impact of various complex factors in real environments, such as atmospheric disturbances, terrain variations, and equipment errors. Therefore, when evaluating the

performance of both positioning algorithms, it is crucial to combine simulation data and empirical data.

In the empirical analysis, this paper again takes the South China Sea chain as an example. By driving the test car, we conducted a detailed investigation across multiple regions. The experimental equipment is shown in Figure 9. The experimental equipment includes an eLoran antenna and receiver, a BeiDou antenna and receiver, and a laptop. The eLoran receiver was modified by the laboratory to accurately output the required time difference (TD) and time of arrival (TOA) data. Its key technical specifications are as follows: it has a reception level range of 30 dB μ V to 114 dB μ V, a noise resistance performance better than -10 dB, a differential range of 0–604 B, a time difference measurement resolution better than 10 ns, and a TOA measurement uncertainty better than 30 ns. The BeiDou receiver has a positioning error within 10 m, and under conditions with no obstructions and minimal external electromagnetic interference, its positioning accuracy can reach within a few meters or even better, providing precise test point location information.



Figure 9. Experimental equipment: (a) eLoran antenna and BeiDou antenna; (b) eLoran receiver and BeiDou receiver.

A modified eLoran receiver was used to receive and process the signals, outputting the corresponding TD and TOA data. Then, the obtained data were processed and analyzed. Finally, the hyperbolic and pseudorange positioning algorithms were applied to solve and compare the final positioning results.

To compare the performance of the two algorithms under different geographic locations and environments, five representative measured points were selected, with their latitude and longitude information provided by the BeiDou receiver. The specific locations of the measured points are shown in Figure 10. The surroundings of each test point were open, with no significant obstructions or other signal interferences. During the tests, the weather was consistently overcast, and the air was slightly humid, which helped maintain consistent experimental conditions.

For each test point, 500 data points were collected and analyzed over a certain period of time, with the mean and standard deviation calculated and presented in Tables 5 and 6. The mean value reflects the overall value of the data during that time period, while the standard deviation reflects the stability of the data during the same period. The average values are consistent with the actual conditions, and the data fluctuations are within a normally acceptable range. TD a represents the difference between the propagation delay of the signal from the Raoping auxiliary station to the receiver and the propagation delay of the signal from the Hezhou main station to the receiver. TD b represents the difference between the propagation delay of the signal from the Chongzuo auxiliary station to the receiver and the propagation delay of the signal from the Hezhou main station to the receiver. TOA a represents the propagation delay of the signal from the Hezhou main

station to the receiver. TOA b represents the propagation delay of the signal from the Raoping auxiliary station to the receiver. TOA c represents the propagation delay of the signal from the Chongzuo auxiliary station to the receiver.

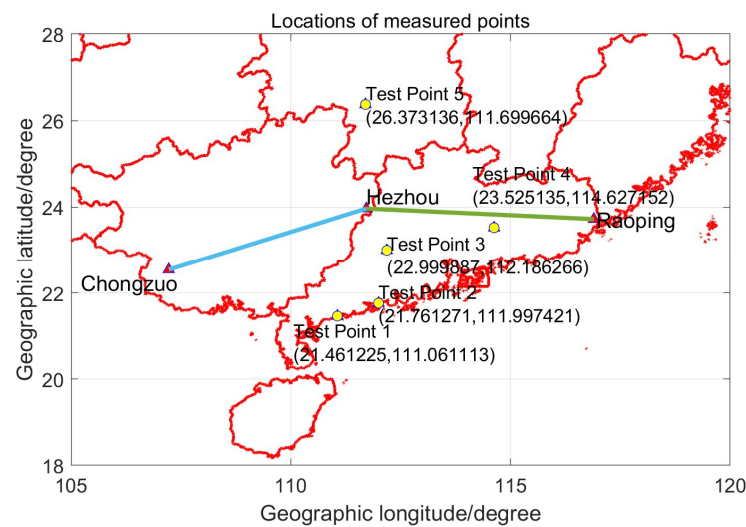


Figure 10. Locations of measured points.

Table 5. Time difference of measured points.

Test Points	TD a		TD b	
	Mean Value (μ s)	Standard Deviation (ns)	Mean Value (μ s)	Standard Deviation (ns)
1	15,681.368	80.4675	27,353.825	71.0576
2	15,473.802	94.2426	27,775.038	248.4493
3	15,704.565	48.7438	28,246.973	20.8909
4	14,237.153	49.1377	28,484.112	50.9635
5	15,582.260	56.8033	28,110.931	18.2817

Table 6. Time of arrival of measured points.

Test Points	TOA a		TOA b		TOA c	
	Mean Value (μ s)	Standard Deviation (ns)	Mean Value (μ s)	Standard Deviation (ns)	Mean Value (μ s)	Standard Deviation (ns)
1	964.521	24.1511	2181.201	80.4489	1392.949	45.4805
2	831.355	15.9152	1840.487	57.4233	1680.837	211.0433
3	401.239	18.0887	1641.078	56.2687	1722.617	27.9710
4	1013.896	26.6440	786.364	39.6652	2572.255	51.3243
5	900.296	15.2866	2017.870	57.1577	2085.700	20.9044

After processing the data, the mean values of the TD and TOA for each measured point were selected and substituted into the algorithms for calculation. The time differences a and b were subtracted from the baseline encoded time delay data of 14,464.6 μ s and 26,925.76 μ s, respectively. The final calculation results are shown in Tables 7 and 8, which list the calculation results and the error information. For ease of analysis, the errors are presented in both degrees and meters, which can be converted between the two units.

Table 7. Positioning error results of the hyperbolic algorithm.

Measured Points	Latitude (°)	Longitude (°)	Latitude Error (°)	Longitude Error (°)	Latitude Error (m)	Longitude Error (m)
1	21.463172	111.059343	0.001947	−0.00177	210.32	−191.186
2	21.767139	111.996913	0.005868	−0.00051	633.75	−54.85
3	23.009498	112.186284	0.009611	0.000018	1037.95	2.00
4	23.553019	114.629526	0.027884	0.002374	3011.43	256.35
5	26.361470	111.700296	−0.011666	0.000632	−1259.93	68.22

Table 8. Positioning error results of the pseudorange algorithm.

Measured Points	Latitude (°)	Longitude (°)	Latitude Error (°)	Longitude Error (°)	Latitude Error (m)	Longitude Error (m)
1	21.463512	111.060021	0.002287	−0.00109	247.01	−117.97
2	21.767441	111.997294	0.00617	−0.00013	666.38	−13.70
3	23.009729	112.186681	0.009842	0.000415	1062.95	44.81
4	23.553083	114.629654	0.027948	0.002502	3018.37	270.22
5	26.360921	111.700960	−0.012215	0.001296	−1319.22	139.94

From Tables 7 and 8, it can be seen that the calculation results of the hyperbolic positioning algorithm and the pseudorange positioning algorithm are generally similar. However, because the data used were uncorrected and directly output by the receiver, they contained significant interference items such as secondary delays and additional secondary delays, resulting in large errors. If these interference items are further corrected, the positioning errors will be significantly reduced. Additionally, Tables 7 and 8 show that the positioning errors at the two coastal measured points are smaller, suggesting that the eLoran system performs better in maritime navigation. In contrast, during land navigation, due to the influence of surrounding terrain and buildings on the signal, larger observational errors were introduced, leading to less accurate positioning.

6. Conclusions

This paper employs a combination of simulation and empirical analysis to deeply study and compare the performance of the hyperbolic positioning algorithm and the pseudorange positioning algorithm.

The simulation analysis evaluates both algorithms in scenarios with and without observational errors. Under conditions without observational errors, by employing a search method to solve for the unknowns and applying suitable convergence thresholds of 10^{-9} degrees for the hyperbolic positioning algorithm and 10^{-11} degrees for the pseudorange positioning algorithm, both algorithms achieved correct positioning across the entire area, with errors being essentially zero; the worst-case error did not exceed 10^{-5} m. The pseudorange positioning algorithm does not require the prior determination of whether the point is in the forward or backward region, and it resolves the singularity problem in the hyperbolic positioning algorithm, thereby improving its practicality in actual applications. Under conditions with observational errors, a detailed analysis of various errors was conducted, and it was found that both algorithms exhibited positioning errors, with the pseudorange algorithm achieving positioning accuracy comparable to that of the hyperbolic algorithm. In the empirical analysis, five typical measured points were selected, and TD and TOA data were collected and processed, which were then input into the algorithms for calculation. The results indicate that the positioning performance of the two algorithms is comparable, validating the simulation conclusions.

The algorithms themselves do not affect positioning accuracy, the factors influencing accuracy are the error terms present in the actual data. In the future, by constructing more

accurate models for secondary time delays and additional secondary time delay estimation errors, it is expected that positioning accuracy can be further improved.

Author Contributions: Conceptualization, M.Y. and B.Y.; methodology, M.Y.; software, M.Y. and B.Y.; validation, M.Y., B.Y. and C.Y.; formal analysis, M.Y. and W.G.; investigation, M.Y.; resources, S.L.; data curation, M.Y.; writing—original draft preparation, M.Y.; writing—review and editing, M.Y. and C.Y.; visualization, M.Y. and C.Y.; supervision, S.L.; project administration, S.L.; funding acquisition, S.L. All authors have read and agreed to the published version of the manuscript.

Funding: This research was funded by the Youth Innovation Promotion Association CAS, grant number: 2021409, funder: Chaozhong Yang.

Data Availability Statement: Restrictions apply to the availability of these data. The ownership of data belongs to the National Time Service Center (NTSC). These data can be made available from the corresponding author with the permission of NTSC.

Acknowledgments: We are grateful to NTSC for providing the necessary resources and facilities that enabled this research. Special thanks go to Shifeng Li for his invaluable guidance and support throughout the project.

Conflicts of Interest: The authors declare no conflicts of interest.

References

1. Xu, B. Research on the development of enhanced Loran navigation technology. *Mod. Navig.* **2019**, *10*, 395–399.
2. Wu, M.; Di, J.; Xu, J.; Li, F. Application and development of eLoran. *Hydrogr. Surv. Charting* **2022**, *42*, 44–49.
3. Son, P.-W.; Rhee, J.H.; Han, Y.; Seo, K.; Seo, J. Preliminary Study of Multichain-based Loran Positioning Accuracy for a Dynamic User in South Korea. In Proceedings of the IEEE/ION Position, Location and Navigation Symposium (PLANS), Monterey, CA, USA, 23–26 April 2018.
4. Son, P.-W.; Rhee, J.H.; Seo, J. Novel Multichain-Based Loran Positioning Algorithm for Resilient Navigation. *IEEE Trans. Aerosp. Electron. Syst.* **2018**, *54*, 666–679. [[CrossRef](#)]
5. Zhang, K.; Wan, G.; Xi, X. Multi-chain positioning algorithm for enhanced Loran system. In Proceedings of the IEEE International Conference on Electron Devices and Solid-State Circuits (EDSSC), Xi'an, China, 12–14 June 2019.
6. Hargreaves, C. ASF Measurement and Processing Techniques, to allow Harbour Navigation at High Accuracy with eLoran. Master's Thesis, University of Nottingham, Nottingham, UK, 2010.
7. Feng, J.; Zhang, S.; Sun, J.; Chen, X.; Xiong, J. Research on joint positioning of Loran-C and astronomical line of position. *Hydrogr. Surv. Charting* **2022**, *42*, 56–59.
8. Kim, H.; Lee, J.; Oh, S.H.; So, H.; Hwang, D.H. Multi-Radio Integrated Navigation System M&S Software Design for GNSS Backup under Navigation Warfare. *Electronics* **2019**, *8*, 188. [[CrossRef](#)]
9. Kim, W.; Son, P.-W.; Rhee, J.H.; Seo, J. Development of Record and Management Software for GPS/Loran Measurements. In Proceedings of the 20th International Conference on Control, Automation and Systems (ICCAS), Busan, Republic of Korea, 13–16 October 2020. [[CrossRef](#)]
10. Liu, Y.; Li, X.; Liu, C.; Zhao, F.; Zhu, F.; Feng, P. The study of systematic error calibration method for Loran-C and GNSS integrated positioning. *J. Time Freq.* **2021**, *44*, 322–330.
11. Liu, Y.; Ren, Y. Optimization of Loran-C and Beidou integrated positioning performance. In Proceedings of the 2020 7th International Conference on Information Science and Control Engineering (ICISCE), Changsha, China, 18–20 December 2020.
12. Chang, S.; Ji, B.; Hu, Q.; Bian, S.; Li, H.; Li, W.; Liu, B. Two algorithms of geodesic line length calculation considering elevation in eLoran systems. *IET Radar Sonar Navig.* **2023**, *17*, 1469–1478. [[CrossRef](#)]
13. Chang, S.; Ji, B.; Wu, M.; Bian, S.; Li, W.; Du, H. Evaluation of Height Correction on Loran Signal's Groundwave Transmission Delay Model. *IEEE Antennas Wirel. Propag. Lett.* **2023**, *22*, 1005–1009. [[CrossRef](#)]
14. Kim, Y.; Fang, T.H.; Kim, D.; Seo, K.; Park, S. Loran-C Multiple Chain Positioning using ToA Measurements. *J. Korean Navig. Port Reserch* **2019**, *43*, 23–32. [[CrossRef](#)]
15. Park, J.; Son, P.-W.; Kim, W.; Rhee, J.H.; Seo, J. Effect of Outlier Removal from Temporal ASF Corrections on Multichain Loran Positioning Accuracy. In Proceedings of the 20th International Conference on Control, Automation and Systems (ICCAS), Busan, Republic of Korea, 13–16 October 2020. [[CrossRef](#)]
16. Zhao, Z.Z.; Liu, J.F.; Zhao, Y.C.; Zhang, J.S.; Song, J.X.; Xi, X.L. Measurement and Analysis of Loran-C Sky Waves throughout the Day. *Electronics* **2024**, *13*, 1240. [[CrossRef](#)]
17. Lebekwe, C.K.; Yahya, A.; Astin, I. An Improved Accuracy Model Employing an e-Navigation System. In Proceedings of the 9th Annual IEEE Ubiquitous Computing, Electronics and Mobile Communication Conference (UEMCON), New York, NY, USA, 8–10 November 2018.
18. Li, Y.; Hua, Y.; Yan, B.R.; Guo, W. Research on the eLoran Differential Timing Method. *Sensors* **2020**, *20*, 6518. [[CrossRef](#)] [[PubMed](#)]

19. Son, P.-W.; Park, S.G.; Seo, K.; Park, S.; Fang, T.H. Preliminary study of the re-radiation effect of Loran signal to improve the positioning accuracy. In Proceedings of the European Navigation Conference (ENC), Warsaw, Poland, 9–12 April 2019. [CrossRef]
20. Gong, C.; Jiang, Z.; Huang, C.; Wang, P.; Wu, T. Optimization Analysis of GDOP of PL-Aided Navigation and Positioning System. In Proceedings of the International Conference on Measurement, Instrumentation and Automation (ICMIA 2012), Guangzhou, China, 15–16 September 2012.
21. Jiang, Y.; Zhong, B.; Wu, M.; Lin, E. Research on Positioning Work Area Based on China loran C System GDOP. In Proceedings of the 2020 IEEE International Conference on Information Technology, Big Data and Artificial Intelligence (ICIBA), Chongqing, China, 6–8 November 2020.
22. Lee, C.-B.; Hoon, Y.S.; Shin, M.Y.; Hwang, S.W.; Lee, S.J. A study on the optimal geometrical placement of eLoran stations in Korea. *J. Korean Navig. Port Res.* **2013**, *37*, 35–40. [CrossRef]
23. Qian, L. Research on Positioning Solution Technology in Loran C Navigation. Master's Thesis, Xi'an University of Electronic Science and Technology, Xi'an, China, 2006.
24. Zhang, B. Research on Positioning Solution Technology of Loran C Receiver. Master's Thesis, Xi'an University of Technology, Xi'an, China, 2022.
25. Yan, B.; Li, Y.; Guo, W.; Hua, Y. A solution method of positioning and timing based on pseudo distance assigning for Loran-C. *J. Time Freq.* **2020**, *43*, 130–142.
26. Liu, K.; Yan, W.; Yuan, J.; Xiao, Z.; Yang, C.; Hua, Y. An Interval Shrinking Trust Region Algorithm for GNSS/eLoran Pseudorange Fusion Positioning Initialization. In Proceedings of the 2022 International Conference on Automation, Robotics and Computer Engineering (ICARCE), Wuhan, China, 16–17 December 2022.
27. Liu, K.Q.; Yuan, J.B.; Yan, W.H.; Yang, C.Z.; Guo, W.; Li, S.F.; Hua, Y. A Shrink-Branch-Bound Algorithm for eLoran Pseudorange Positioning Initialization. *Remote Sens.* **2022**, *14*, 1781. [CrossRef]
28. Liu, J.; Zhu, Y.; Li, B. Research on non-time-based cross-circle positioning method for Loran C system. *Ship Electron. Eng.* **2011**, *31*, 64–68.
29. Yan, B.; Li, Y.; Guo, W.; Hua, Y. High-Accuracy Positioning Based on Pseudo-Ranges: Integrated Difference and Performance Analysis of the Loran System. *Sensors* **2020**, *20*, 4436. [CrossRef] [PubMed]
30. SJ 20839-2002; Computational Method of L-W Ground-Wave Transmission Channels. China Electronics Standardization Institute: Beijing, China, 2003. Available online: <https://max.book118.com/html/2019/0910/5340224133002124.shtml> (accessed on 21 August 2024).

Disclaimer/Publisher's Note: The statements, opinions and data contained in all publications are solely those of the individual author(s) and contributor(s) and not of MDPI and/or the editor(s). MDPI and/or the editor(s) disclaim responsibility for any injury to people or property resulting from any ideas, methods, instructions or products referred to in the content.